Materials & Design 249 (2025) 113545

Contents lists available at ScienceDirect

Materials & Design

journal homepage: www.elsevier.com/locate/matdes

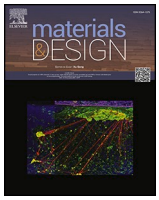

Die geometry influence on the texture and microstructure development during extrusion of AZ31 and ZK60 magnesium alloy chips

Leo Hendriok [a,*], Maria Nienaber [b], Gerrit Kurz [b], Noomane Ben Khalifa [a,b]

[a] Institute for Production Technology and Systems, Leuphana University Lüneburg, Universitätsallee 1, 21335 Lüneburg, Germany
[b] Institute of Material and Process Design, Helmholtz-Zentrum Hereon, Max-Planck-Str. 1, 21502 Geesthacht, Germany

ARTICLE INFO

Keywords:
Solid-state recycling
Chip extrusion
Magnesium alloy
Texture
ECAP
EBSD

ABSTRACT

Solid state recycling by direct extrusion of metal chips can significantly reduce energy requirements in comparison to traditional recycling strategies and primary production. The process consists of cold-compacting the chips into chip-based billets and subsequent hot extrusion to the desired profile. Thereby, mechanical properties comparable to conventional profiles made from as-cast billets can be achieved. This study examines the development of microstructure and texture and their impact on the mechanical properties. Consequently, extrusion experiments are conducted using two sets of dies, namely a flat face (FF) die and an ECAP die, with magnesium alloys AZ31 and ZK60. The texture of the profiles and extrusion remainders of both dies is measured using EBSD and XRD in order to analyse the influence of the chips and deformation path on the texture development. The microstructure of the extruded chip-based profiles exhibits notable grain refinement, which can be attributed to the substantial mechanical strain introduced during milling and compaction of the chips. Furthermore, it is demonstrated that the combination of chip-based billets and FF die extrusion results in a favourable weakening of basal texture and development of a RE-like < 2–1-11 > texture component, thus causing a tilt of basal planes out of extrusion direction. Conversely, ECAP extrusion leads to an increased intensity of basal texture, highlighting the influence of deformation path on texture development. Finally, it is shown that a combination of microstructure and texture effects can result in preferable mechanical properties of chip-based profiles.

1. Introduction

The use of magnesium for structural components is motivated by its high strength-to-weight ratio and thus its suitability for lightweight applications. A reduction of weight can significantly reduce energy consumption and carbon emissions during the product service time, especially in the mobility sector. Nevertheless, energy requirement for the production of primary magnesium is high, resulting in high carbon emissions. Alternatively, secondary magnesium can be used as a substitute by recycling magnesium scrap material. Different strategies can be found in literature of which solid-state recycling (SSR) by hot extrusion proves to be capable of further reducing energy consumption and carbon emissions due to omitting melting of the scrap material [1]. SSR is suitable especially for recycling of scrap material with high surface-to-volume ratio such as milling chips due to avoidance of melting losses which can result from the high amount of oxides [2].

Several studies on the extrusion of magnesium chips show the feasibility of mechanical properties comparable or even higher than profiles from as-cast billets [3,4]. This improvement of mechanical properties is mostly attributed to the amount and dispersion of oxide particles and the resulting grain refinement due to increased nucleation rate [5,6]. It was shown that the increased pressure, strain and shear through die design can lead to improved welding of aluminium alloy chips [7]. Especially severe plastic deformation processes such as ECAP improve the mechanical properties during SSR [8]. The effect of high strain during extrusion of magnesium alloys was demonstrated by Chino et al. [9] by a high extrusion ratio of 1600:1 resulting in more uniformly distributed oxide particles and subsequently improved strength through grain refinement and dispersion strengthening. Ying et al. [10] showed that the combination of extrusion and ECAP leads to improved tensile strength of chip-based AZ91 magnesium alloy profiles, even though the basal texture is weakened, which is attributed to grain refinement by dispersed oxides. A weakened basal texture after ECAP of isothermal sintered Mg-RE chips was also observed by Pei et al. [11] leading to an improved ductility of the sample. In general, ECAP is known to be an efficient tool for production of ultra-fine grain Mg-alloy structures with

* Corresponding author.
E-mail address: leo.hendriok@leuphana.de (L. Hendriok).

https://doi.org/10.1016/j.matdes.2024.113545
Received 12 September 2024; Received in revised form 7 December 2024; Accepted 12 December 2024
Available online 13 December 2024

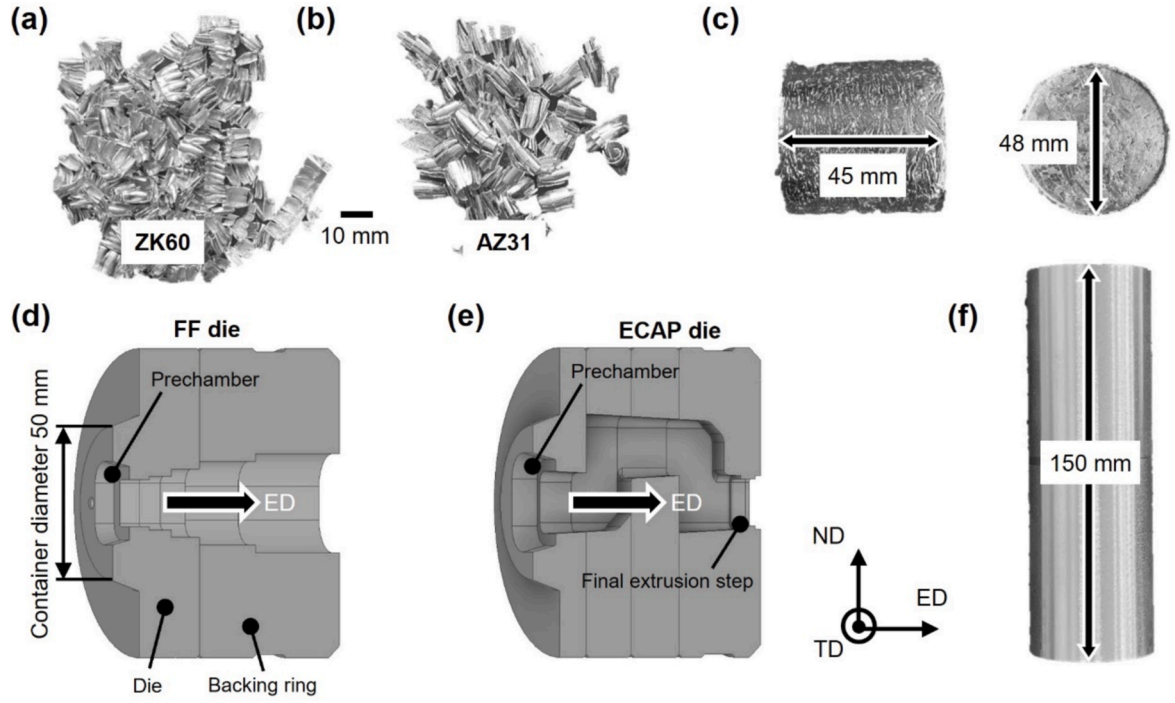

Fig. 1. chip geometry of ZK60 chips (a) and AZ31 chips (b), chip-based billet after cold compaction of AZ31 chips (c) and respective reference billet (f). The flat face (FF) die (d) and ECAP die (e) used for the extrusion experiments.

improved mechanical properties [12]. Furthermore ECAP can lead to weakening of the texture and formation of texture favourable for basal slip without lowering strength [13,14].

It is well known that texture plays a major role in determining the formability of magnesium alloys due to the hexagonal crystal lattice and limited slip systems [15]. The texture is thereby influenced by parameters such as extrusion speed, temperature, deformation history and initial texture [16,17].

Nevertheless, no study was found that analyses the texture development during solid-state recycling of ZK60 and AZ31 magnesium alloy chips by extrusion. Therefore, this paper will systematically investigate the texture modification induced by the chip material and through different strain paths introduced by die design. The findings provide crucial information to further improve the properties of solid-state recycled Mg-alloy chips by connecting the texture and microstructure characteristics to the mechanical properties.

2. Methods

The materials used in this work consist of chip-based billets as well as conventional extrusion billets (referred to as reference billets) made from cast magnesium alloy AZ31 (3 wt% Al, 1 wt% Zn, 0.4 wt% Mn) and extruded ZK60 (5.16 wt% Zn, 0.072 wt% Zr). Homogenization was done at 400 °C for 16 h to eliminate local differences in concentration of alloying elements and thus ensure homogeneous material properties of the reference billets. To produce the chip-based billets three consecutive steps were carried out. Firstly, the chips were produced by turning and milling from the as-received billets of the alloys ZK60 and AZ31 respectively resulting in chip geometries as shown in Fig. 1 (a, b). To ensure clean chips, turning and milling was performed omitting lubricants. Subsequently, chip-based billets were produced by cold-compaction to simplify handling and to increase the relative density thereby increasing yield (Fig. 1c).

Due to the high friction between the chips and compaction container, cold compaction was realised in portions of 120 g with a compaction pressure of 240 MPa to ensure mechanical bonding of the chips, resulting in billets of approx. 45 mm length and a relative density of approx. 84 %.

Extrusion experiments were carried out on a 2.5 MN extrusion press of Müller Engineering. Two different dies were used (Fig. 1d and 1e). A normal flat face (FF) die and in order to increase pressure, strain and shear on the material a variation of an ECAP die was used. The presented ECAP-die slightly tapers towards the die exit ensuring die filling. Nevertheless, a high amount of strain by shearing in the intersection between ECAP-channels is still present. Both dies depicted produce profiles with a rectangular cross section with a side length of 15 mm and a corner radius of 1.5 mm. This results in an extrusion ratio of $R = 8.67$ for both the FF and ECAP die. Extrusion was carried out at 350 °C and a ram speed of 1 mm/s. Billets were preheated to 350 °C for one hour. All of the specimens for testing were taken from the mid-section of the profile to ensure steady state of the extrusion process.

Compression tests were performed in accordance with DIN 50106 at room temperature. The tests were done strain-controlled with a strain rate of 0.001 s-1 at RT on a Zwick Z050 universal testing machine. Stress strain curves were recorded and the mechanical properties such as compression yield stress (CYS), ultimate compression stress (UCS) and fracture strain were determined. Cylindrical compression specimen of the dimensions $h = 13.5$ mm and $d = 9$ mm were produced resulting in a height to diameter ratio of 1.5. Both, tests with specimen in extrusion direction (ED) as well as in normal direction (ND) were performed to investigate anisotropic effects of the profiles in respect to mechanical properties. For each condition three tests were carried out in order to take statistical deviations into account. From each of the three tests one curve was selected to show the behaviour of the specimen of each condition exemplarily.

The microstructure of all profiles was observed by optical light microscopy. Therefore, the samples were ground to size, polished using SiC paper from #800 to #2500 and further polished using a diamond suspension and oxide polishing suspension (OPS). After polishing the specimens were etched in a picric acid solution, according to Kree et al. [18], to make the grain boundaries visible for microscopy. The solution consists of 10 ml distilled water, 150 ml ethanol, 7 ml acetic acid and 6 g of picric acid. The etching process was carried out for 3–5 s. The microstructure shown in the following depicts the ED-TD-plane.

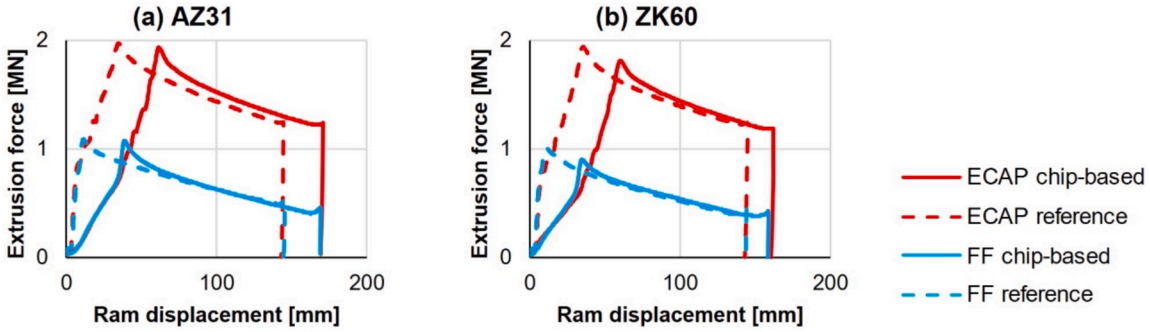

Fig. 2. Extrusion force diagrams for AZ31 (a) and ZK60 specimens (b) extruded at 350 °C and 1 mm/s for both dies (FF and ECAP) and both billet types (solid and chip-based).

EBSD (electron backscatter diffraction) measurements were carried out on a Zeiss Ultra 55 with an acceleration voltage of 15 kV and a step size of 0.6 μm. To analyse the grain orientation of the samples inverse pole figures (IPFs), which depict the texture components of the basal planes (0001) and the first- (10–10) and second-order (2–1-10) prismatic planes as well as grain orientation maps were calculated using TSL OIM Analysis 7. The preparation of the samples follows the scheme of optical testing by light microscopy without etching. The resulting sample corresponds to the ED-TD plane of the centre of the profile. In addition to mechanical polishing, the samples were electropolished using an AC2 solution (StruersTM) at 30 V and −20 °C for 40 s to further remove fine scratches.

Global texture of the initial materials was measured by an X-ray diffractometer (PANalytical X'Pert PRO MRD). Additionally, texture in different locations of the remaining discard and profile was measured to gain insights into the texture development during extrusion through the FF and ECAP die. Inverse pole figures (IPF) were calculated using open-source code MTEX [19].

An FE-model was set up in *QForm UK Extrusion* to analyse the influence of strain path, i.e. extrusion die on the temperature fields. The model was created using the Extrusion mode which allows for mechanically and thermally coupled simulations of material flow and die deformation. A built in material model for AZ31 was used based on [20]. Friction is calculated by Levanov Law with Friction factor 1 and Levanov coefficient 1.25 [21]. The extrusion parameters were chosen in accordance with the experimental setup. The model was validated against the extrusion force with a deviation of 8.67 % and 3.33 % for the ECAP and FF die respectively.

3. Results and Discussion

3.1. Extrusion force and extrusion temperature

The extrusion force of the conducted experiments, extruded at 350 °C and 1 mm/s ram speed, is shown in Fig. 2 as a function of ram displacement. The results are similar between AZ31 and ZK60, with the maximum extrusion force being slightly higher for AZ31 than for ZK60. All curves show a smoothly declining force after reaching the peak indicating a good extrudability of both chip-based and reference billets. The comparison between the flat-face (FF) and ECAP die shows that almost double the force is needed to extrude using the ECAP die which indicates a higher resulting pressure affecting the chips. Additionally, the pre-chamber and ECAP turns are observable in the curves by the force reaching a plateau and then further increasing. Comparison of the force–displacement curves of the reference and chip-based billets shows a distinction in the force increasement. Whereas the force during extrusion of the reference billet increases rapidly during upsetting inside the container, the rate of increasement of the force of the chip-based billet is lower, as it is further compacted rather than upset inside the container. This results in a larger ram displacement as well. Furthermore, a slightly lower maximum extrusion force can be seen for the chip-based billets. Which can be related to differences in billet length after fully compacting the billet inside the container and thus a lower friction force. Due to the long extrusion channel and the ECAP turns, the high forming and friction forces demand for a higher extrusion force.

The temperature calculated by means of FEM is depicted in Fig. 3. The maximum temperature during the process is given for each die for the last calculated step corresponding to the extrusion of the whole

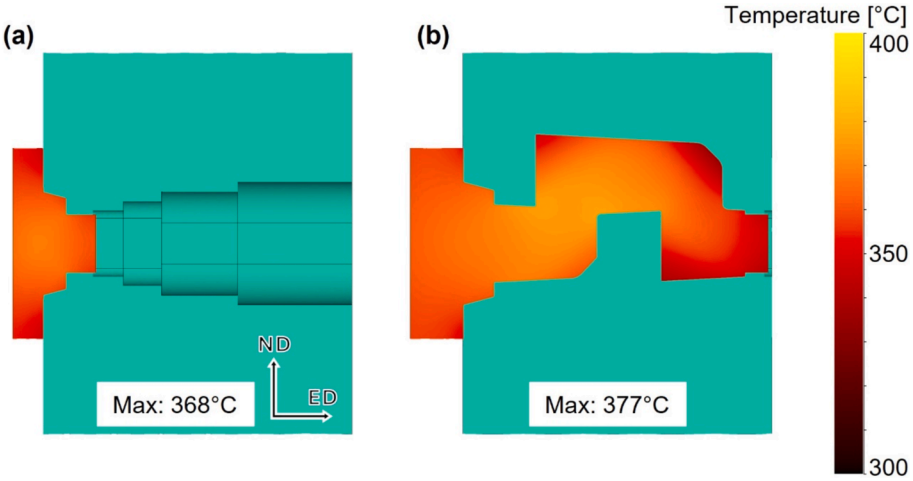

Fig. 3. Temperature calculated by QForm UK Extrusion for the FF (a) and ECAP (b) die during extrusion of AZ31 billets with a ram speed of 1 mm/s and process temperature of 350 °C.

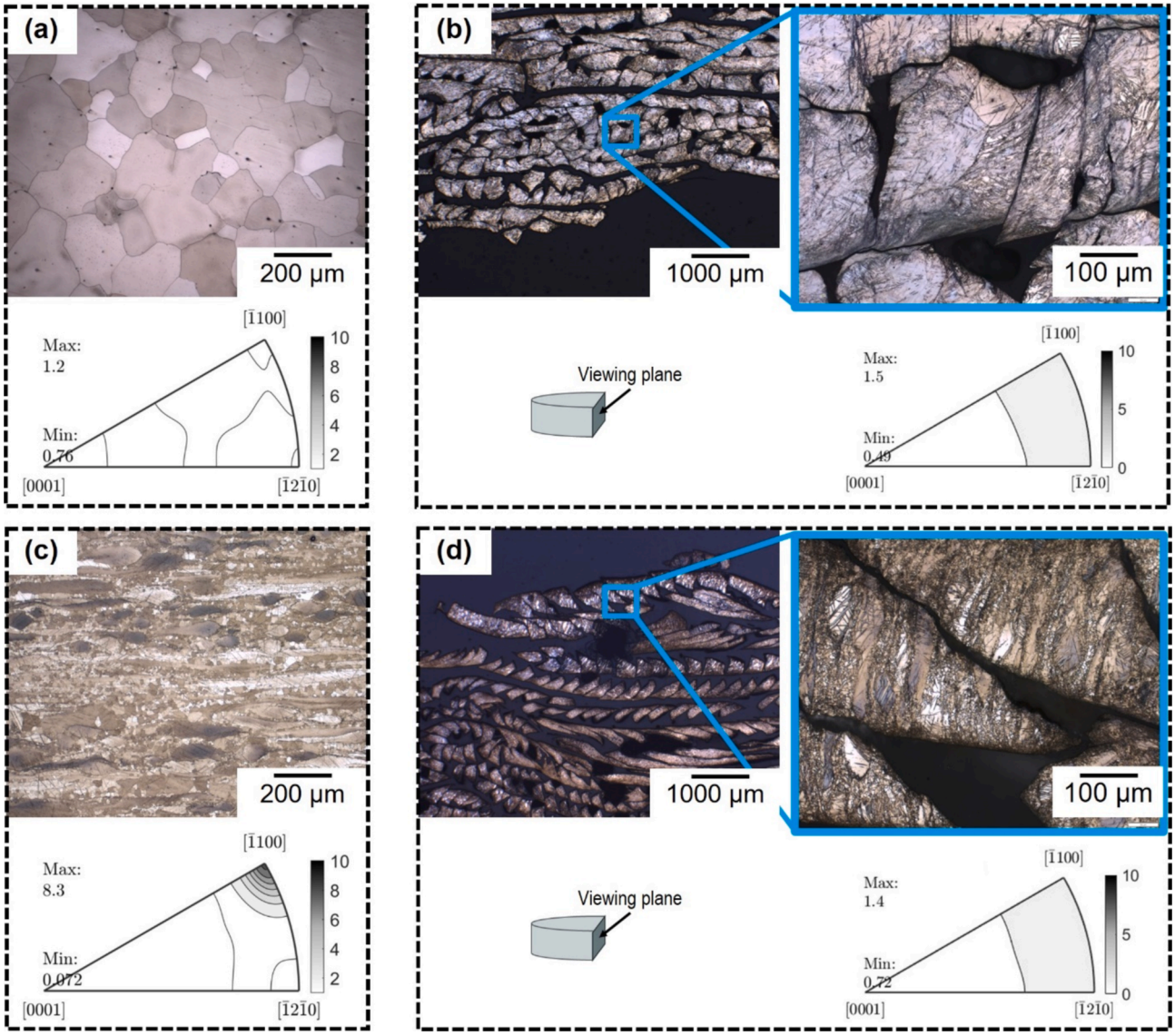

Fig. 4. Microstructure and texture of the reference AZ31 billet (a), reference ZK60 billet (c), compacted AZ31 chip-based billet (b), and compacted ZK60 chip-based billet (d).

billet. The maximum temperature is 368 °C and 377 °C for the FF- and ECAP-die respectively. The maximum temperature of the FF dies is located in the primary forming zone while the maximum temperature during extrusion through the ECAP die can be located at the corner of the first ECAP turn.

3.2. Microstructure

Fig. 4a shows the microstructure of the as-cast AZ31 billet. Large equiaxed grains can be seen. Fig. 4b shows the microstructure of the cold compacted AZ31 billet. Chips are clearly visible and metal to metal contact between chips is only partly established. It shows that each chip consists of multiple loosely connected chip fragments. Taking a closer look into the microstructure of each chip fragment a high amount of twins are visible. Moreover, the bonding of chips after cold compaction is enabled by mechanical interlocking, no welding is visible.

In Fig. 4c the microstructure of the ZK60 reference billet is shown. It can be seen that the microstructure differs significantly from the AZ31 reference billet due to the production of the reference material by extrusion. The difference can mainly be seen in a deformation microstructure consisting of elongated and small recrystallized grains. Furthermore, large, elliptical grains are visible. The microstructure of the chip-based ZK60 billet is depicted in Fig. 4d and consists of overall smaller grains compared to the chip-based AZ31 billet. Nevertheless, similar to the chip-based AZ31 billet a high number of twins can be seen.

The microstructure of the specimens in ED-TD-plane is depicted in Fig. 4. The AZ31 ECAP reference specimen (Fig. 5b) shows a heterogeneous microstructure with mostly equiaxed grains. Additionally, isolated unevenly shaped grains that are elongated in ED are visible. The respective chip-based specimen (Fig. 5f) shows mostly fine equiaxed grains with some areas of larger grains. Chip boundaries are well visible by aligned grain boundaries, differences in grain size, and scattered particles along those boundaries. The reference specimen of the FF-die (Fig. 5a) shows a microstructure interspersed by in ED elongated grains. In between, bands of smaller equiaxed grains can be found parallel to ED. The chip-based AZ31 specimen of the FF die (Fig. 5e) shows a mostly homogenous microstructure of small equiaxed grains. Differences in grain size in-between chips are less pronounced compared to the chip-based ECAP specimen. Chip boundaries are visible by particles located between chips and aligning grain boundaries.

All specimens of the alloy ZK60 (Fig. 5c,d,g,h) are characterized by elliptical grains elongated in ED surrounded by smaller equiaxed grains.

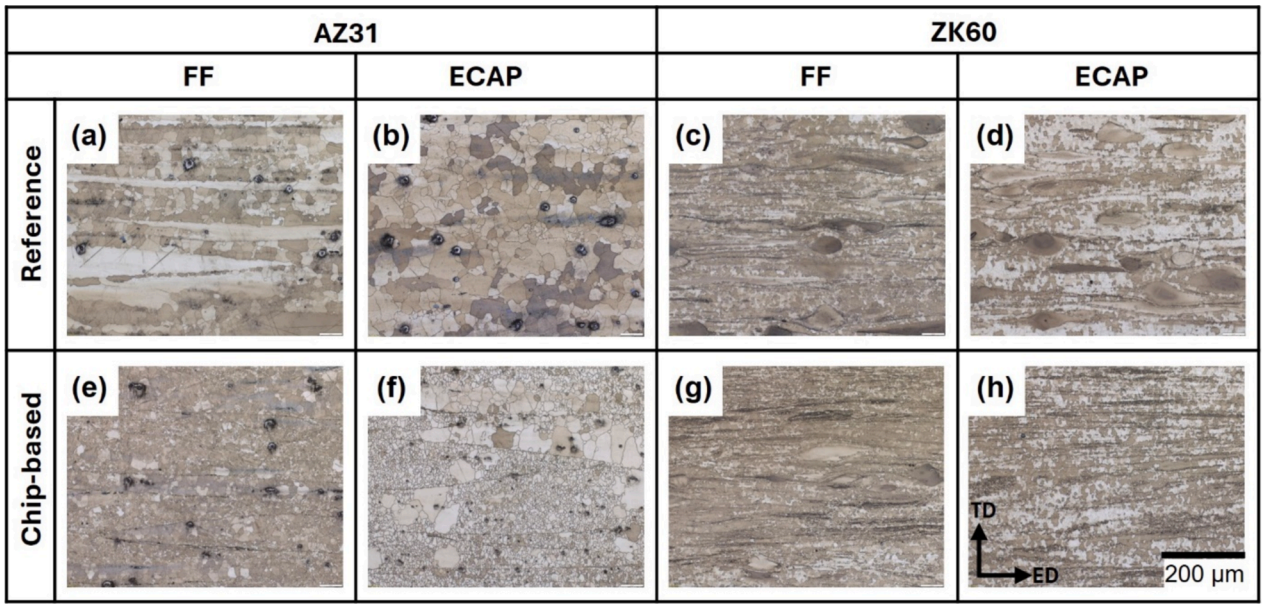

Fig. 5. Microstructure of the extruded AZ31 specimens (a,b and e,f) and ZK60 specimens (c,d and g,h).

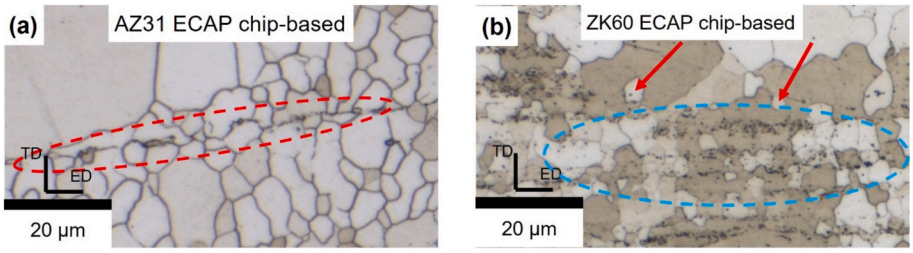

Fig. 6. Microstructure of the AZ31 chip-based ECAP specimen (a). The red dashed line indicates the chip boundary and oxide particles. Microstructure of the ZK60 chip-based ECAP specimen (b). Zone of fine grains and high number of particles is indicated by blue dashed line. Island grains are indicated by red arrows. (For interpretation of the references to colour in this figure legend, the reader is referred to the web version of this article.)

The amount of elliptical grains seems to be higher in the reference specimens (FF and ECAP die) and the lowest amount can be seen in the chip-based ECAP specimen. Overall, the chip-based specimens appear to have smaller grains than their respective reference specimen.

Overall, ZK60 specimens show a refined microstructure compared to AZ31 specimens. In contrast to the particles being located along chip boundaries in the recycled AZ31 specimens (Fig. 6a), there are particles visible in both recycled and reference specimens in the ZK60 alloy that are dispersed in the microstructure.

Additionally, the microstructure of the ZK60 specimens differentiates from the AZ31 specimens through elliptical grains along ED. These elliptical grains are mainly found in the reference samples, while they are only occasionally visible in the chip-based samples. This microstructure may be attributed to Zr-rich cores found in ZK60 alloys, which only partly recrystallize during extrusion [22]. Dependent on the imposed strain during extrusion those cores recrystallize into areas of fine grains or form elongated unrecrystallized grains along ED. In other words, a higher strain leads to a higher degree of recrystallization [23]. Since the chip-based specimens undergo high straining during the milling process and during cold-compaction before being extruded the amount of recrystallized Zr-rich cores is higher compared to reference specimens. This can further contribute to the grain refinement as seen in the chip-based specimens of the ZK60 alloy.

As seen in the microstructure a reduction of grain size correlates with the use of chip-based billets instead of the reference billets. Consequently, the use of chip-based billets leads to smaller grains in comparison to reference billets independent of the used extrusion die. Similar findings can be found in literature that connect the grain refinement in connection with solid-state recycling of magnesium alloy chips to impeded grain growth through dispersed oxide particles. [9,10]. As shown in Fig. 6b, a high concentration of particles corresponds to smaller grains in the chip-based ZK60 ECAP specimen indicating impeded grain growth and particle stimulated nucleation (PSN). PSN can have a significant influence on the microstructure of ZK60 alloys by promoting dynamic recrystallization through posing as nucleation sites for new grains [24]. This can contribute to the grain refinement of ZK60 specimens in general. The oxide particles of the chip-based AZ31 specimens are mainly located on the chip surfaces. That is, a grain refining effect of particles is unlikely for AZ31 as no dispersion of particles is visible (see Fig. 6a). Nevertheless, it can be seen that the chip boundaries lead to impeded grain growth as is visible through the aligned grain boundaries along the chip boundaries of the chip-based AZ31 specimens.

Furthermore, the initial microstructure of the chip-based billets consists of a high number of twins compared to the as-cast microstructure caused by machining and cold-compaction prior to extrusion (Fig. 4b,d). Deformation twins are known to facilitate the nucleation of new grains during dynamic recrystallization and result in a fine-grained microstructure [25]. Therefore, it is likely that the fine-grained microstructure of the chip-based specimens results from extensive twinning prior to extrusion. Thereby, the high number of twins leads to a high nucleation rate during DRX during extrusion, leading to a fine-grained microstructure as seen in the chip-based specimens.

Against expectations, the use of an ECAP die does not lead to further

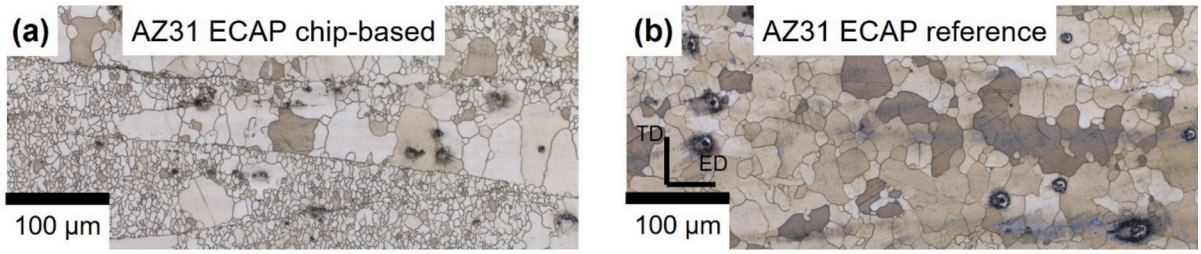

Fig. 7. Bimodal microstructure of AZ31 chip-based and reference ECAP specimens. Large and small grains are separated by chip boundaries in the chip-based specimen (a) and interspersed in the reference specimen (b).

grain refinement neither for chip-based specimens nor for reference specimens. On the contrary, the use of the ECAP die leads to larger grains, particularly for the AZ31 specimens. The difference in grain size of the specimens of the ZK60 alloy is less pronounced. The microstructure of the AZ31 ECAP specimens shows differentiating features between chip-based and reference specimens. While the chip-based specimen has a clear separation between areas of large and small grains through the chip's boundaries, see Fig. 7a, the microstructure of the reference specimen shows no such separation. Instead, small grains are scattered in between larger grains, see Fig. 7b.

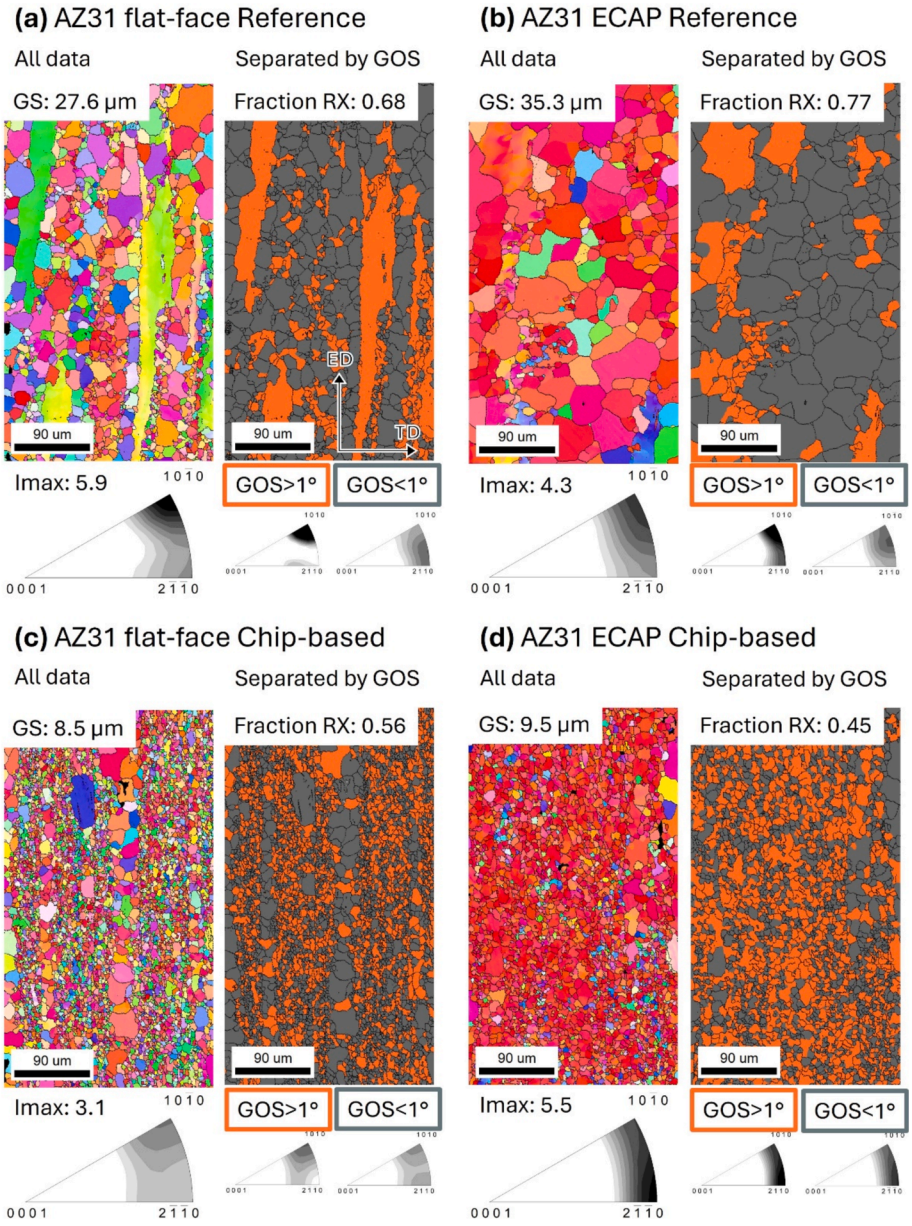

Fig. 8. EBSD maps and IPFs of reference and chip-based AZ31 specimens extruded through ECAP and FF die. Separation of microstructure by grain orientation spread (GOS).

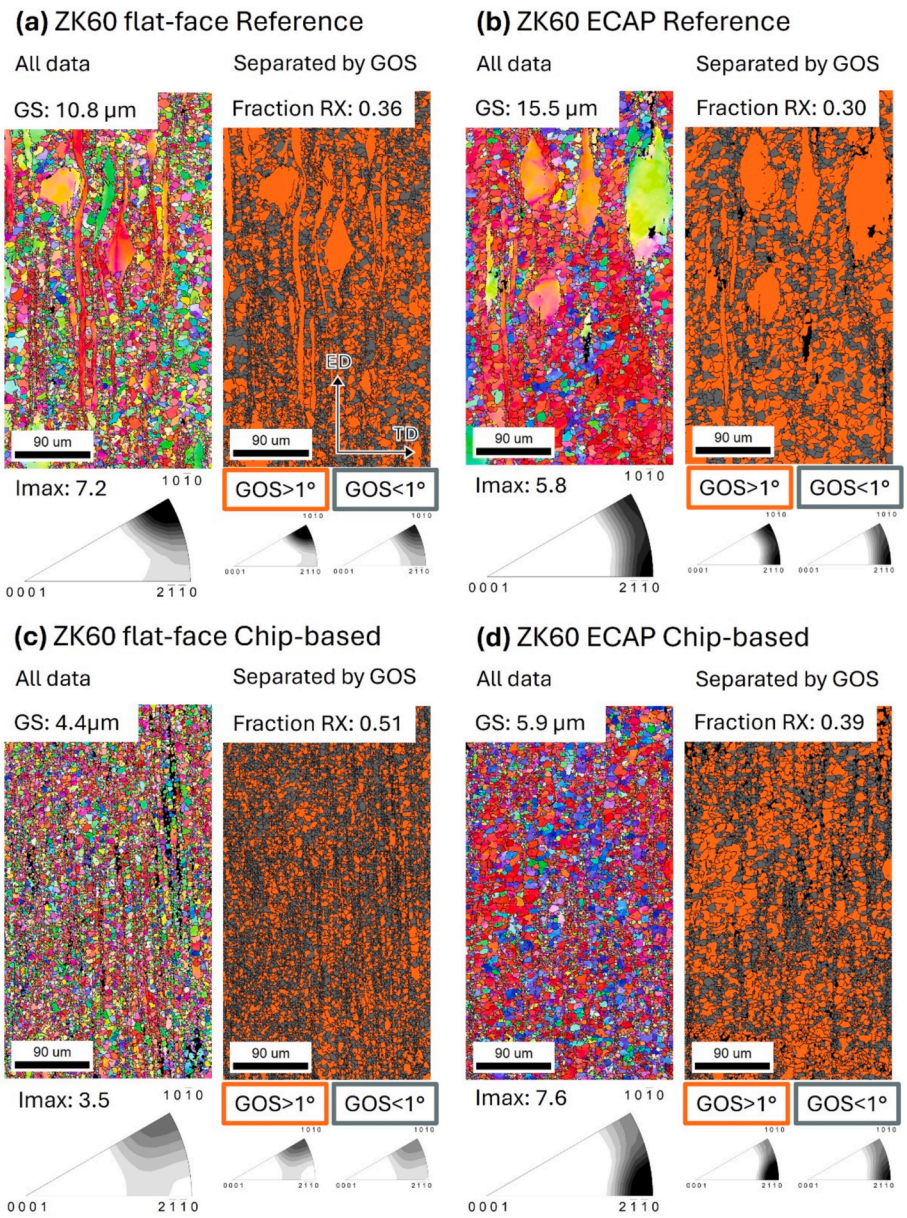

Fig. 9. EBSD maps and IPFs of reference and chip-based ZK60 specimens extruded through ECAP and FF die. Separation of microstructure by grain orientation spread (GOS).

This bimodal grain size distribution in connection with severe plastic deformation through ECAP can be associated with abnormal grain growth (AGG). AGG is further characterized by the presence of "island grains" and is reportedly taking place during annealing of highly strained metals [26,27]. Instead of homogenous grain growth during recrystallization some grains grow rapidly, leading to a coarse heterogeneous microstructure. The characteristic island grains can be seen exemplarily in Fig. 6 (red arrows) of the microstructure of the ZK60 ECAP chip-based specimen but also occur in the other ECAP specimens. Different explanations for AGG can be found in literature differentiating between the effect of second phase particles, differences in crystallographic orientations and differences in stored energy of grains [27–29].

The high strain induced into the material during ECAP can result in a temperature instability of the microstructure [30]. Subsequently, differences in stored strain can lead to selective grain growth during annealing of highly strained metals, such as ECAPed magnesium sheets [27]. In general, a minimum annealing temperature must be exceeded for AGG to take place [31]. It is important to note that due to cooling of the profiles in air, slow cooling rates can be expected. Thus, two mechanisms need to be considered for the resulting microstructure, those are DRX and SRX. Even though, no annealing in the traditional sense is carried out, the high temperature of the profile is maintained, possibly leading to temperature activated recrystallization without further deformation (SRX). This is further promoted by the high amount of strain induced during extrusion and incomplete DRX. Additionally, the irregular distribution of chips leads to a randomized orientation of grains in the chip-based billets. Dependent on the orientation of grains relative to the load direction during extrusion different degrees of deformation affect the chips. This might influence dynamic recrystallization and thus lead to differences in grain size in-between chips.

Furthermore, nonuniformly distributed second phase particles can lead to locally impeded grain growth and a locally lower pinning force respectively and thus resulting in heterogenous grain size distributions [28]. This effect is also found in extruded nano-TiC/AZ61 bars due to a nonuniform distribution of nano particles [32]. In respect to chip-based specimens this could mean a locally higher pinning force through oxide

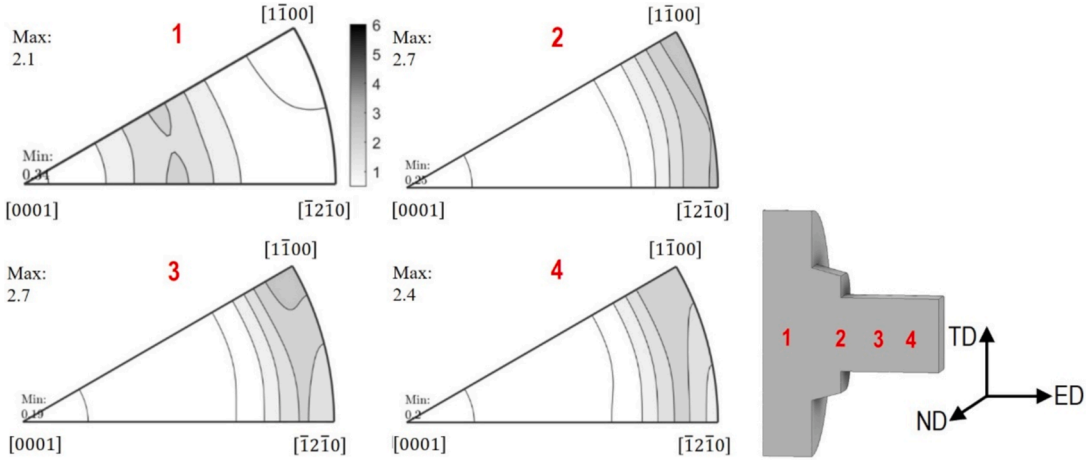

Fig. 10. IPFs of the AZ31 chip-based FF profile and discard before the first extrusion step (1), during the extrusion step (2) and after the extrusion step (3, 4). The development of a characteristic deformation texture can be seen.

particles along the chip's surfaces, resulting in the bimodal microstructure of the chip-based AZ31 specimen (Fig. 5 e,f). A similar effect of AGG in chip-based specimens at high extrusion ratios was observed by Chino et al. [9] but attributed to a uniform dispersion of oxide particles during extrusion with high extrusion ratios. However, since no oxides can be seen dissolving from the chip boundaries to the inside of the chips in the AZ31 specimens this effect seems to be unlikely (Fig. 6a).

3.3. Texture

The texture of the initial material is shown in Fig. 4. The cast AZ31 reference billet is characterized by a random texture distribution (Fig. 4a). The ZK60 reference billet shows a < 10–10 > -component corresponding with the highly deformed microstructure. Additionally, a weak < -12–11 > component is visible. The texture of the chip-based billets of both alloys is similar, consisting of a weak orientation of basal planes in direction of the cold compaction (Fig. 4b,d).

Fig. 8 shows orientation maps from EBSD and as a separation tool grain orientation spread (GOS) maps with the corresponding IPFs of the AZ31 specimens. A bimodal microstructure of in ED elongated grains and small equiaxed grains with average GS = 27.6 μm is visible in the FF reference specimen, Fig. 8a. A preferred orientation of basal planes parallel to ED is apparent in the FF reference specimen with double-fibre along the arc between the < 10–10>- and the < 11–20 > -poles, whereas the < 10–10 > fibre component is more pronounced. By considering a grain orientation spread GOS > 1° (assuming that recrystallized grains have low internal misorientation [33]), the elongated grains show to be deformed and non-recrystallized. The texture for GOS greater than 1 shows the well-known deformation texture (<10–10>- component) in the nonrecrystallized microstructure. Similarly, the ECAP reference specimen shows a bimodal grain structure (GS: 35.3 μm) with large inhomogeneously formed non-recrystalized grains, Fig. 8b. Also here, the double-fibre along the arc between the < 10–10>- and the < 11–20 > -poles, with a higher intensity towards the < 10–10 > pole, dominates the texture. Comparing the chip-based (Fig. 8 c,d) with the reference specimen (Fig. 8 a,b), it is apparent that the grain size is much smaller in the chip-based specimens with an average GS of 8.5 μm and 9.5 μm for the FF and ECAP die respectively. Both chip-based specimens show a bimodal microstructure with mostly small equiaxed grains but areas of larger equiaxed grains arranged in bands along ED. In contrast to the reference specimen of the FF die, the chip-based specimen shows a weakened RE-like texture component. So, a texture with tilt of basal planes out of the extrusion direction. A rotation of the texture similar to RE-textures as described by Standford et al. [34]. Whereas the highest intensity is also at the < 10–10 > pole. It is important to note that this RE texture is already clearly present in the non-recrystallised grain structures (GOS greater than 1°). However, the IPF of the chip-based ECAP specimen shows a more intense texture with the previously mentioned component for the reference samples (double-fibre) Fig. 8d. In contrast, the maximum intensity is visible towards < 2–1-10 > instead of < 10–10 > of the reference specimen. The fraction of recrystallized grains differs from reference to chip-based specimens and in-between FF and ECAP die. While the reference ECAP specimen has the highest RX fraction (0.77) the chip-based ECAP specimen has the lowest (0.45). Both chip-based specimens have a lower fraction of recrystallized grains than their respective reference specimen.

Fig. 9 shows the grain orientation maps and corresponding IPFs of the ZK60 specimen. Compared to the chip-based specimen the pronounced elliptical and elongated grains are well noticeable in the reference specimen. The grain orientation map shown in Fig. 9 with GOS < 1° indicates those grains as deformed but not recrystallized. Similar to the AZ31 specimens, the reference specimens of the ZK60 alloy have a higher average grain size. However, the difference is less pronounced than for the AZ31 alloy. Again, a slightly higher average GS is visible in the ECAP specimens compared to the FF specimens. The FF reference specimen exhibits a < 10–10 > fibre component. In contrast, the ECAP reference specimen shows a double-fibre along the arc between < 10–10 > and < 2–1-10 > poles with the highest intensity towards the latter. Equally to the AZ31 specimen, the ZK60 FF chip-based specimen shows a weakened RE-like texture component. Again, this RE texture is already clearly present in the non-recrystallised grain structures. On the other hand, the chip-based ECAP specimen shows a texture similar to the respective reference specimen, but with a more pronounced fibre component towards the < 2–1-10 > pole.

The chip-based ZK60 specimens show, in contrast to the AZ31 specimens, a higher fraction of recrystallized grains compared to their respective reference specimen. The highest fraction is reached by the FF chip-based specimen (0.51). That is, the ZK60 specimens show a mainly deformed microstructure.

Typically, a basal texture forms during extrusion whereby different fibre components develop dependent on processing parameters [17,35]. The most common < 10–10 > fibre component, which forms during extrusion or drawing of rods and wires [36,37], can be seen in both reference specimens extruded through the FF die. The use of chip-based billets (FF extrusion) instead leads to a weakening and broadening of the texture and significant reduction of grain size. It can be hypothesized that both effects result from the high amount of twins found in the compacted billets caused by high straining during machining of the chips and the cold-compaction process. It is important that this texture modification only exists in the chip-based FF specimens but not the FF

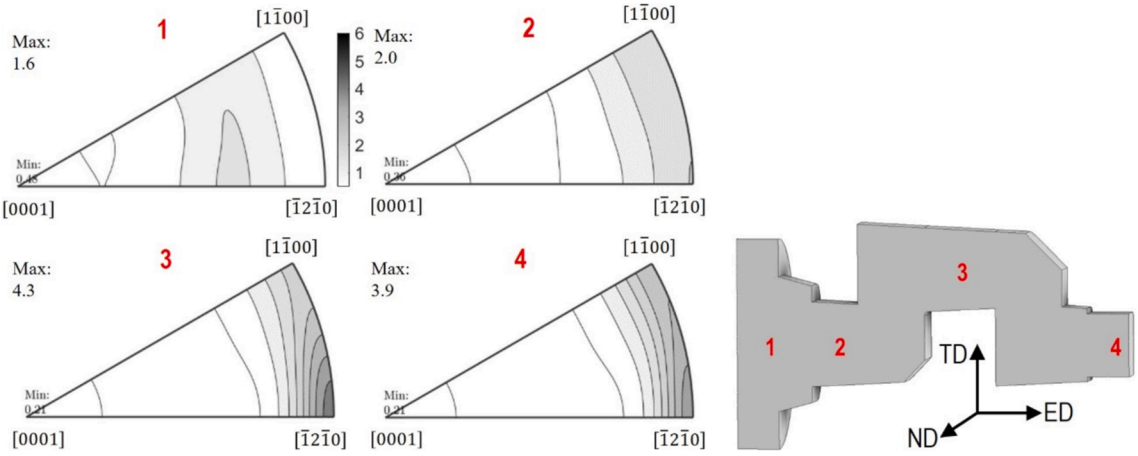

Fig. 11. IPFs of the AZ31 chip-based ECAP profile and discard before reaching the first extrusion step (1), after the first extrusion step (2), after the first two ECAP turns (3) and after the final extrusion step (4).

specimens made from reference billets. This excludes the possibility of a rigid rotation causing the RE-like texture component. Instead, it must be induced by the chip material. It can therefore be assumed that the low intensity texture of the chip-based extrudates is connected to the randomized pre-texture of the chip-based billets and high number of twins in combination with the RE-like texture of the deformed microstructure the weak characteristic texture of the chip-based specimens forms.

The effect of a weakened / tilted texture is visible for both alloys extruded through the FF die (chips) but is more pronounced for the ZK60 alloy. The AZ31 specimen loses the < 2–1-10 > component and the < 10–10 > fibre is weakened, while the ZK60 specimen develops a component similar to RE-alloys [34]. The IPFs in Fig. 8c and 9c show that the RE-component is mainly introduced by the deformed grains and already present in the initial ZK60 microstructure (Fig. 4c). In addition to the RE-texture of the deformed microstructure, a weakened texture is also visible in the recrystallized microstructure of the chip-based FF specimen. On top of grain refinement due to extensive twinning and DRX as described in Zhu and Ringer [25], recrystallized grains originating from twins can result in a weakened, non-basal texture [38]. Thus, the high amount of twinning introduced during machining and cold-compaction of the chips can explain the reduced texture intensity of the chip-based FF specimens. However, no such relationship can be seen for the ECAP specimens, thus, indicating the influence of deformation path on texture development.

Table 1
Grain size (GS) and mechanical propertiescompression yield stress (CYS), ultimate compression stress (UCS) and fracture strain from compression tests in ED and ND of the chip-based and reference AZ31 and ZK60 specimens.

Alloy	Direction	Die/ condition	CYS	UCS	Fracture strain	GS
			MPa	MPa	%	µm
AZ31	ED	FF reference	94 ± 1	398 ± 1	10.7 ± 0.2	27.6
		FF chip-based	141 ± 2	419 ± 3	11.4 ± 0.1	8.5
		ECAP reference	82 ± 0	377 ± 5	8.6 ± 0.5	35.3
		ECAP chip-based	123 ± 3	399 ± 7	7.7 ± 0.4	9.5
	ND	FF reference	86 ± 2	326 ± 2	13.5 ± 0.2	
		FF chip-based	135 ± 7	359 ± 4	12.7 ± 0.9	
		ECAP reference	87 ± 24	344 ± 25	11.6 ± 3.5	
		ECAP chip-based	198 ± 7	369 ± 3	3.6 ± 0.3	
ZK60	ED	FF reference	160 ± 3	461 ± 2	7.6 ± 0.1	10.8
		FF chip-based	192 ± 3	458 ± 14	9.6 ± 0.7	4.4
		ECAP reference	161 ± 6	473 ± 8	8.8 ± 0.6	15.5
		ECAP chip-based	192 ± 3	455 ± 6	9.4 ± 0.6	5.9
	ND	FF reference	139 ± 1	396 ± 4	12.1 ± 0.3	
		FF chip-based	171 ± 4	396 ± 16	10.3 ± 1.4	
		ECAP reference	155 ± 31	382 ± 53	7.9 ± 4.1	
		ECAP chip-based	191 ± 1	342 ± 13	4.9 ± 0.1	

3.4. Texture development

To gain insight on the influence of deformation path on the development of texture XRD measurements were carried out in different positions on the remaining discard and profile. The measurements were carried out on the AZ31 ECAP and FF chip-based extrusion remainders. Fig. 10 shows the positions of measurements and corresponding IPFs of the AZ31 FF chip-based specimen. Depending on the location of measurement different textures are visible. Moreover, three distinctive zones of similar texture can be recognized. In detail, position 1 features a weakened basal texture with a tilt of approximately 40° towards ED. Position 1 corresponds to the remaining discard before reaching the prechamber. During the final extrusion step a double fibre running along the arc between < -12–10 > and < 1–100 > poles forms (position 2) which concentrates towards a single fibre at the < 1–100 > pole at the die exit (position 3). However, a deflection of the basal planes in ED can already be recognised in position 3. In position 4, after exiting the die a further weakening of the texture and deflection of basal planes towards the ED is visible which develops into a double-fibre component with a slight tilt of the basal planes towards ED (position 4).

Texture development along the deformation path during ECAP can be seen in Fig. 11. While the remaining discard shows a similar texture as the FF die discard (position 1), the first extrusion step leads to an alignment of basal planes along ED (position 2). After the first two ECAP turns the texture develops into a double fibre along the arc between < -12–10 > and < 1–100 > poles but with its highest intensity towards the former (Position 3). The texture after the final extrusion step (position 4) is similar to position 3. The slight reduction in intensity in position 4 can be set into the context of recrystallization. As shown by Jin et al. [39], the fraction of DRXed grains increases after exiting the die, leading to a reduced grain size and decreased intensity of texture.

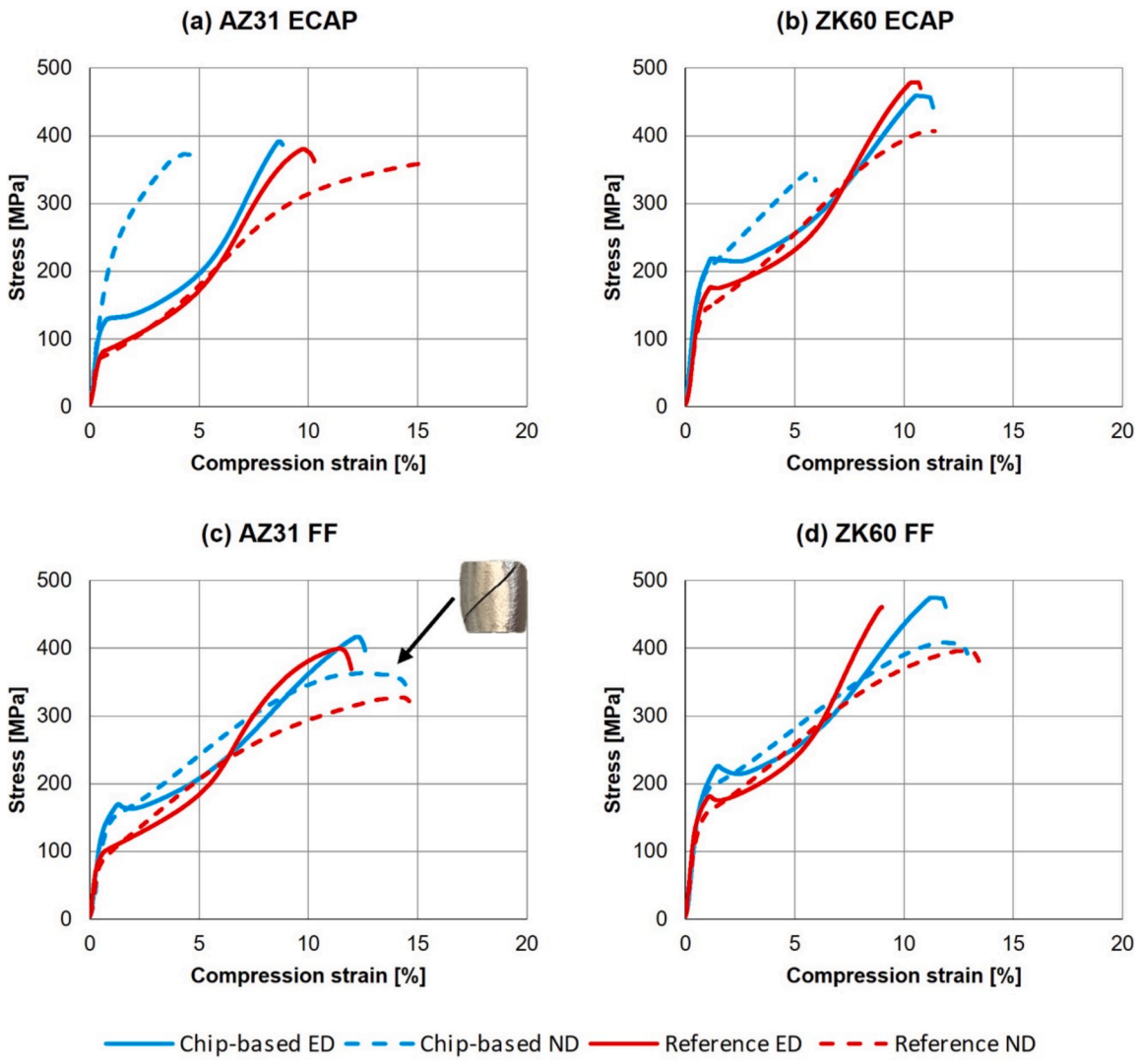

Fig. 12. Compression test diagrams (strain controlled 0.001 s^{-1}).

The resulting texture measured by XRD after the final extrusion step (Figs. 10 and 11, position 4) matches with the texture measured by EBSD (Fig. 8c and 8d).

While in Fig. 10 position 3 on the FF discard shows a characteristic < 1–100 > deformation component (additional to the weak RE-component), this component weakens in position 4 after exiting the die. The IPFs in Fig. 8c show that the RE-like texture component is part of the deformed microstructure. With progressing recrystallization, the < 1–100 > deformation component is diminished. The weak recrystallization texture and formation of the RE-texture can again be set into context of the high amount of twins present in the chip-based billets, as described in Section 3.3. As shown in Nienaber et al. [40] twins lead to a realignment of grains. A significant texture weakening due to a randomization of the orientation distribution has been explained by locally pronounced twin reorientations. Also, Peng et al. [41] reveal that texture weakening was produced by (10–11) twins related to static recrystallization.

The texture of the ECAP die in position 2 shows a weak texture, comparable to the FF die in position 4. This is before reaching the first ECAP turn. The texture in position 4 is then comparable to the texture measured by EBSD. It was shown that the deformation texture is comparable to the overall texture of the profile (Fig. 8d). Therefore, it can be concluded that the deformation path is responsible for differences in texture development, namely the high intensity double fibre of the ECAP die. Additionally, it can be shown that the weakened recrystallization texture introduced by the chips gets diminished. Instead, a typical recrystallization component towards the < -12–10 > pole forms.

3.5. *Effect of microstructure and texture on mechanical properties*

The results of the compression tests (Table 1) are depicted in Fig. 12 as stress–strain-curves. Generally, the curves follow the behaviour of ductile materials. None of the compression specimens show signs of delamination indicating sufficient bonding of the chips. Furthermore, the fractures occur close to a 45° angle to the compression direction. In ED the UCS is reached by the chip-based FF specimen (419 MPa) in case of AZ31 and the reference ECAP specimen (473 MPa) for ZK60. Furthermore, the chip-based specimens of the alloy AZ31 show a higher UCS value than the reference specimen of the respective die.

The chip-based ECAP specimens of both alloys show a deviating curve in ND with a significantly lower fraction strain indicating a more brittle behaviour. While the AZ31 chip-based ECAP specimen still reaches high UCS, the ZK60 chip-based ECAP specimen has lower values compared to the other specimens.

More significant differences are visible for the CYS with a higher value for all chip-based specimen compared to the reference specimen of the respective die. Additionally, a lower yield strength is visible in the AZ31 ECAP specimens compared to the FF specimens, with exception of

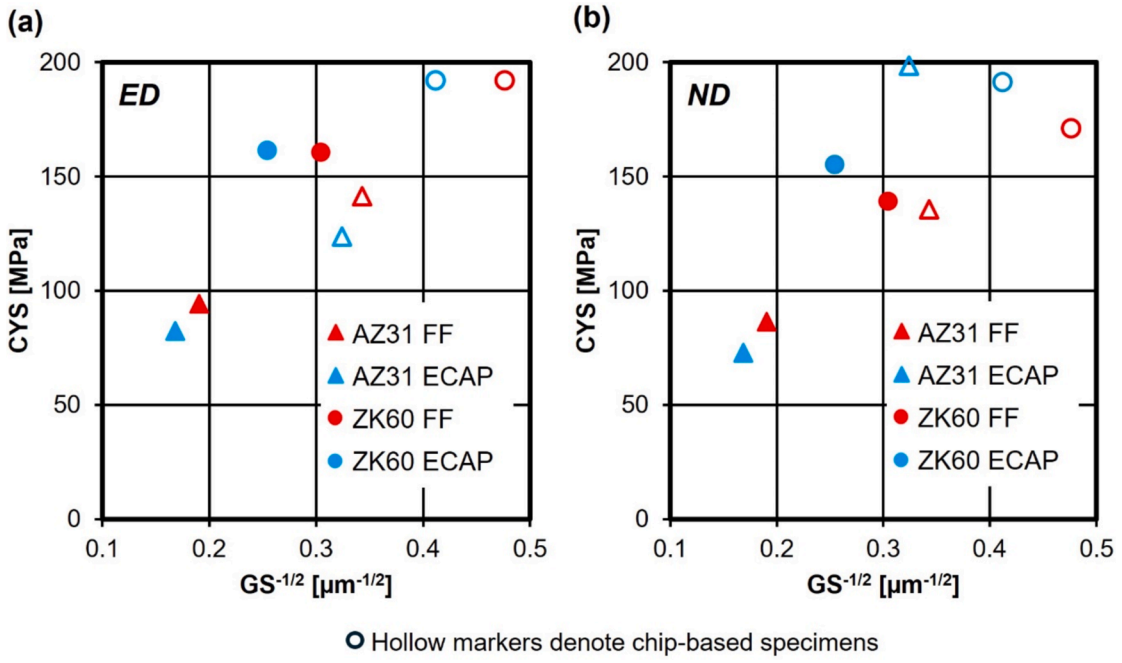

Fig. 13. Hall-Petch relation with grain size values generated from EBSD measurements in (a) ED and (b) ND.

the before mentioned chip-based ECAP specimen in ND. Contrasting, there is no such relation visible in the ZK60 specimens, instead yield strength in ED is only dependent on condition of the billet not on the used die. Moreover, in ND the ECAP specimens show higher yield strength than the respective FF specimen.

The welding of chips during solid-state recycling is primarily prevented by oxide layers covering the chips surfaces, which hinder metal to metal contact being established [42]. The oxide layers of magnesium alloy chips form as porous, brittle, and thin layers, which are easy to break up. Thus, comparably low levels of pressure are needed during extrusion to enable micro-extrusion through gaps of the oxide layers. Since pressure during extrusion is mainly introduced through extrusion ratio and die design, sufficient welding of the chips is feasible already at low extrusion ratios. This can be seen in the mechanical properties of the chip-based specimen of the FF die, which reach values comparable to or even exceeding the reference specimen in compression strength and ductility despite comparably low extrusion ratio of R = 8.76. Furthermore, no delamination of the deformed compression specimen is visible (Fig. 12), indicating sufficient welding of the chips, even at low extrusion ratios.

The development of mechanical properties can be connected to mechanisms such as grain refinement and texture. Especially grain refinement is known to be the main mechanism contributing to improvements of mechanical properties of hcp-alloys [43]. The improvement of mechanical properties of solid-state recycled magnesium chips is also reported in literature and connected to grain refinement and particle-dispersion strengthening [9,10]. This increasement is attributed to oxides being finely dispersed by severe deformation which results in impeded grain growth and particle-dispersion strengthening [9]. In order to analyse the effect of grain refinement on the Hall-Petch relation is plotted in Fig. 13, by setting the CYS in relation to grain size. The linear dependency of the parameters CYS and GS can be given by the following equation [44,45]:

$$\sigma_y = \sigma_0 + kd^{-1/2} \quad (1)$$

Where σ_y is the yield stress (CYS), σ_0 is the friction stress for dislocation gliding along slip planes and k is the Hall-Petch factor. In good agreement with the Hall-Petch relation, an increase in CYS with refined microstructure is noticeable for both alloys in ED (Fig. 13a). Therefore, the improved mechanical properties can mainly be attributed to grain refinement. Nevertheless, differences in the slope and friction stress of the Hall-Petch relation are obvious between the different alloys. Different factors such as texture, grain size and deformation temperature are known to have significant influence on those parameters. Thus, the two parameters grain size and texture must be taken into account in analysing the different Hall-Petch slopes. While a decreasing grain size is known to reduce the slope [46], an increase in texture results in higher Hall-Petch parameters [47]. The results given by Fig. 13a show that the higher texture intensity ZK60 has a higher friction stress but lower k value. This can be explained by the combined effect of GS and texture effecting the Hall-Petch slope. The higher friction stress can be attributed to the higher texture intensity while the lower slope can be related to conflicting effects of overall lower GS leading to a reduced slope but higher texture increasing the slope. Meanwhile, the lower GS and texture intensity of the AZ31 specimens leads to lower friction stresses and higher slope of the Hall-Petch relation. The yield strength in ND in dependency of GS is given in Fig. 13b. The results show lower consistency with the Hall-Petch-relationship compared to ED. This highlights the importance of texture effects on mechanical properties and their anisotropy.

Overall, texture plays a decisive role in determining the mechanical properties and their anisotropy, due to the limited slip system available in magnesium alloys [48]. A weakening of texture and tilt of basal planes away from ED results in increased ductility and decrease of yield and ultimate stresses [49]. On the one hand, an increasement of ductility of the chip-based FF specimens which show a weakened basal texture can be seen. On the other hand, no decreases in strength are visible which can be related to the refined microstructure of those specimens, as shown by the Hall-Petch-Relation in Fig. 13.

Additionally, a distinctive deformation behaviour is visible for the chip-based ECAP specimens when comparing ND to ED, resulting in a significantly lower ductility. This behaviour is especially pronounced for both chip-based specimen. Since anisotropy of hcp materials is primarily introduced through texture effects [50], this behaviour can be attributed to the increased texture intensity of the ECAP specimens compared to FF specimen. That is, the high intensity basal texture leads to a more difficult activation of the basal slip system and thus resulting in the

lower compression limit. Additionally, the ECAP chip-based specimens of the AZ31 and ZK60 alloy show a low fraction of recrystallized grains (0.45 and 0.39). In other words, the dislocation density is high resulting in work hardening and thus in a significantly lower ductility and higher CYS, as seen in the respective AZ31 specimen.

4. Summary and Conclusion

In this work, the solid-state recycling by hot extrusion of AZ31 and ZK60 magnesium alloy chips was analysed. In particular, the influence of the chips and the influence of the tool path on microstructure and texture development was studied. It was shown that the resulting profiles from directly recycled chips have mechanical properties comparable to those of profiles made from solid billets.

- The grain refinement of chip-based profiles can be attributed to the high amount of twins induced during milling and cold compaction. This results in the formation of fine SRX grains during processing.
- Against expectations, no grain refinement is visible by ECAP extrusion.
- The chip-based profiles extruded through the FF die show the formation of a RE-like texture component and weakening of the basal texture. This is again related to the highly twinned microstructure of the chip-based billet resulting in a randomization of texture through locally pronounced twin reorientations and a weakening of basal structures during RX.
- In contrast, the ECAP die leads to an increased intensity of basal texture of the chip-based specimens. It was shown that the increased texture intensity first appears after the first ECAP turn. Thus, this can be attributed to repetitive shear during ECAP.
- The mechanical properties can be related to a combinatory effect of grain refinement and texture. Overall, the improvement in strength can be attributed to grain refinement as shown by the Hall-Petch-relation. On the one hand, the distinctive behaviour of ECAP specimens, namely a significantly lower ductility, results from the high intensity basal texture induced during the ECAP process. The high ductility of the chip-based FF specimens on the other hand, can be attributed to the RE-like texture component.

CRediT authorship contribution statement

Leo Hendriok: Writing – original draft, Visualization, Validation, Methodology, Investigation, Conceptualization. **Maria Nienaber:** Writing – original draft, Visualization, Validation, Methodology, Investigation, Conceptualization. **Gerrit Kurz:** Writing – review & editing, Methodology. **Noomane Ben Khalifa:** Writing – review & editing, Supervision, Resources, Methodology, Funding acquisition, Conceptualization.

Declaration of competing interest

The authors declare that they have no known competing financial interests or personal relationships that could have appeared to influence the work reported in this paper.

Acknowledgements

The project “TrICo - Transformation through Innovation and Cooperation in Communities” was funded by the Federal Ministry of Education and Research under grant number 03IHS284A. The author is responsible for the content of this publication. The authors would like to thank Mr. Alexander Reichart for his help during experimental trials.

Data availability

The raw/processed data required to reproduce these findings cannot be shared at this time as the data also forms part of an ongoing study.

References

[1] J.R. Duflou, A.E. Tekkaya, M. Haase, T. Welo, K. Vanmeensel, K. Kellens, W. Dewulf, D. Paraskevas, Environmental assessment of solid state recycling routes for aluminium alloys: Can solid state processes significantly reduce the environmental impact of aluminium recycling? CIRP Annals 64 (2015) 37–40, https://doi.org/10.1016/j.cirp.2015.04.051.
[2] Y. Xiao, M. Reuter, Recycling of distributed aluminium turning scrap, Miner. Eng. 15 (2002) 963–970, https://doi.org/10.1016/S0892-6875(02)00137-1.
[3] M. Mabuchi, K. Kubota, K. Higashi, New Recycling Process by Extrusion for Machined Chips of AZ91 Magnesium and Mechanical Properties of Extruded Bars, Mater. Trans., JIM 36 (1995) 1249–1254, https://doi.org/10.2320/matertrans1989.36.1249.
[4] Y. Chino, R. Kishihara, K. Shimojima, H. Hosokawa, Y. Yamada, C. Wen, e, H. Iwasaki, M. Mabuchi, Superplasticity and Cavitation of Recycled AZ31 Magnesium Alloy Fabricated by Solid Recycling Process, Mater. Trans. 43 (2002) 2437–2442.
[5] S. Wu, Z. Ji, T. Zhang, Microstructure and mechanical properties of AZ31B magnesium alloy recycled by solid-state process from different size chips, J. Mater. Process. Technol. 209 (2009) 5319–5324, https://doi.org/10.1016/j.jmatprotec.2009.04.002.
[6] M. Hu, Z. Ji, X. Chen, Z. Zhang, Effect of chip size on mechanical property and microstructure of AZ91D magnesium alloy prepared by solid state recycling, Mater. Charact. 59 (2008) 385–389, https://doi.org/10.1016/j.matchar.2007.02.002.
[7] V. Güley, A. Güzel, A. Jäger, N. Ben Khalifa, A.E. Tekkaya, W.Z. Misiolek, Effect of die design on the welding quality during solid state recycling of AA6060 chips by hot extrusion, Mater. Sci. Eng., A 574 (2013) 163–175, https://doi.org/10.1016/j.msea.2013.03.010.
[8] M. Haase, N. Ben Khalifa, A.E. Tekkaya, W.Z. Misiolek, Improving mechanical properties of chip-based aluminum extrudates by integrated extrusion and equal channel angular pressing (iECAP), Mater. Sci. Eng., A 539 (2012) 194–204, https://doi.org/10.1016/j.msea.2012.01.081.
[9] Y. Chino, T. Hoshika, J.-S. Lee, M. Mabuchi, Mechanical properties of AZ31 Mg alloy recycled by severe deformation, J. Mater. Res. 21 (2006) 754–760, https://doi.org/10.1557/jmr.2006.0090.
[10] T. Ying, M. Zheng, X. Hu, K. Wu, Recycling of AZ91 Mg alloy through consolidation of machined chips by extrusion and ECAP, Trans. Nonferrous Met. Soc. China 20 (2010) s604–s607, https://doi.org/10.1016/S1003-6326(10)60547-X.
[11] Y. Pei, H. Ma, M. Yuan, B. Teng, Solid state recycling of Mg–Gd–Y–Zn–Zr alloy chips by isothermal sintering and equal channel angular pressing, J. Magnesium Alloys (2022), https://doi.org/10.1016/j.jma.2022.11.007.
[12] A. Yamashita, Z. Horita, T.G. Langdon, Improving the mechanical properties of magnesium and a magnesium alloy through severe plastic deformation, Mater. Sci. Eng., A 300 (2001) 142–147, https://doi.org/10.1016/S0921-5093(00)01660-9.
[13] W. Kim, S. Hong, Y. Kim, S. Min, H. Jeong, J. Lee, Texture development and its effect on mechanical properties of an AZ61 Mg alloy fabricated by equal channel angular pressing, Acta Mater. 51 (2003) 3293–3307, https://doi.org/10.1016/S1359-6454(03)00161-7.
[14] D. Orlov, G. Raab, T.T. Lamark, M. Popov, Y. Estrin, Improvement of mechanical properties of magnesium alloy ZK60 by integrated extrusion and equal channel angular pressing, Acta Mater. 59 (2011) 375–385, https://doi.org/10.1016/j.actamat.2010.09.043.
[15] T. Al-Samman, G. Gottstein, Room temperature formability of a magnesium AZ31 alloy: Examining the role of texture on the deformation mechanisms, Mater. Sci. Eng., A 488 (2008) 406–414, https://doi.org/10.1016/j.msea.2007.11.056.
[16] X. Huang, K. Suzuki, Y. Chino, M. Mabuchi, Influence of initial texture on rolling and annealing textures of Mg–3Al–1Zn alloy sheets processed by high temperature rolling, J. Alloys Compd. 537 (2012) 80–86, https://doi.org/10.1016/j.jallcom.2012.05.002.
[17] Q. Liu, X. Zhou, H. Zhou, X. Fan, K. Liu, The effect of extrusion conditions on the properties and textures of AZ31B alloy, J. Magnesium Alloys 5 (2017) 202–209, https://doi.org/10.1016/j.jma.2017.03.002.
[18] V. Kree, J. Bohlen, D. Letzig, K.U. Kainer, Metallographische Gefügeuntersuchungen von Magnesiumlegierungen, Prakt. Metallogr. 41 (2004) 233–246.
[19] F. Bachmann, R. Hielscher, H. Schaeben, Texture Analysis with MTEX – Free and Open Source Software Toolbox, Solid State Phenom. 160 (2010) 63–68, https://doi.org/10.4028/www.scientific.net/SSP.160.63.
[20] L. de Pari Jr, W.Z. Misiolek, J.H. Forsmark, A.A. Luo, Flow stress modeling for large strain deformation in magnesium alloy AZ31, Comput Mat Sci 10 (2010) 108–129.
[21] A. Levanov, Improvement of metal forming processes by means of useful effects of plastic friction, Journal of Materials Processing Technology 72 (1997) 314–316, https://doi.org/10.1016/S0924-0136(97)00191-X.
[22] M. Shahzad, L. Wagner, The role of Zr-rich cores in strength differential effect in an extruded Mg–Zn–Zr alloy, J. Alloys Compd. 486 (2009) 103–108, https://doi.org/10.1016/j.jallcom.2009.06.123.
[23] M. Shahzad, L. Wagner, Microstructure development during extrusion in a wrought Mg–Zn–Zr alloy, Scr. Mater. 60 (2009) 536–538, https://doi.org/10.1016/j.scriptamat.2008.12.006.
[24] P. Peng, K. Zhang, J. She, A. Tang, J. Zhang, K. Song, Q. Yang, F. Pan, Role of second phases and grain boundaries on dynamic recrystallization behavior in ZK60 magnesium alloy, J. Alloys Compd. 861 (2021) 157958, https://doi.org/10.1016/j.jallcom.2020.157958.

[25] S.Q. Zhu, S.P. Ringer, On the role of twinning and stacking faults on the crystal plasticity and grain refinement in magnesium alloys, Acta Mater. 144 (2018) 365–375, https://doi.org/10.1016/j.actamat.2017.11.004.
[26] J. Dennis, P.S. Bate, J.F. Humphreys, Abnormal Grain Growth in Metals, Mater. Sci. Forum 558–559 (2007) 717–722, https://doi.org/10.4028/www.scientific.net/MSF.558-559.717.
[27] J. Victoria-Hernández, J. Suh, S. Yi, J. Bohlen, W. Volk, D. Letzig, Strain-induced selective grain growth in AZ31 Mg alloy sheet deformed by equal channel angular pressing, Mater. Charact. 113 (2016) 98–107, https://doi.org/10.1016/j.matchar.2016.01.002.
[28] P.R. Rios, Abnormal grain growth development from uniform grain size distributions in the presence of stable particles, Scr. Mater. 39 (1998) 1725–1730, https://doi.org/10.1016/S1359-6462(98)00370-4.
[29] H.-C. Kim, C.-G. Kang, M.-Y. Huh, O. Engler, Effect of primary recrystallization texture on abnormal grain growth in an aluminum alloy, Scr. Mater. 57 (2007) 325–327, https://doi.org/10.1016/j.scriptamat.2007.04.023.
[30] J. Stráská, M. Janeček, J. Čížek, J. Stráský, B. Hadzima, Microstructure stability of ultra-fine grained magnesium alloy AZ31 processed by extrusion and equal-channel angular pressing (EX–ECAP), Mater. Charact. 94 (2014) 69–79, https://doi.org/10.1016/j.matchar.2014.05.013.
[31] D. Raabe, Recovery and Recrystallization: Phenomena, Physics, Models, Simulation, in: D.E. Laughlin, K. Hono (Eds.), Physical Metallurgy, Elsevier, 2015, pp. 2291–2397.
[32] L. Fan, M. Zhou, W. Lao, Y. Zhang, H. Dieringa, Y. Zeng, Y. Huang, G. Quan, Improving the ductility and toughness of nano-TiC/AZ61 composite by optimizing bimodal grain microstructure via extrusion speed, J. Magnesium Alloys (2023), https://doi.org/10.1016/j.jma.2023.02.011.
[33] M. Nienaber, J. Bohlen, S. Yi, G. Kurz, K.U. Kainer, D. Letzig, Influence of Ca addition on the dynamic and static recrystallization behavior of direct extruded flat profiles of Mg-Y-Zn alloy, J. Magnesium Alloys 11 (2023) 3736–3748, https://doi.org/10.1016/j.jma.2023.09.017.
[34] N. Stanford, M.R. Barnett, The origin of “rare earth” texture development in extruded Mg-based alloys and its effect on tensile ductility, Mater. Sci. Eng., A 496 (2008) 399–408, https://doi.org/10.1016/j.msea.2008.05.045.
[35] M.G. Jiang, C. Xu, H. Yan, G.H. Fan, T. Nakata, C.S. Lao, R.S. Chen, S. Kamado, E. H. Han, B.H. Lu, Unveiling the formation of basal texture variations based on twinning and dynamic recrystallization in AZ31 magnesium alloy during extrusion, Acta Mater. 157 (2018) 53–71, https://doi.org/10.1016/j.actamat.2018.07.014.
[36] I.L. Dillamore, W.T. Roberts, Preferred orientation in wrought and annealed metals, Metall. Rev. 10 (1965) 271–380, https://doi.org/10.1179/mtlr.1965.10.1.271.
[37] M. Nienaber, M. Braatz, N. Ben Khalifa, J. Bohlen, Property profile development during wire extrusion and wire drawing of magnesium alloys AZ31 and ZX10, Mater. Des. 224 (2022) 111355, https://doi.org/10.1016/j.matdes.2022.111355.
[38] D. Guan, W.M. Rainforth, B. Le Ma, J.G. Wynne, Twin recrystallization mechanisms and exceptional contribution to texture evolution during annealing in a magnesium alloy, Acta Mater. 126 (2017) 132–144, https://doi.org/10.1016/j.actamat.2016.12.058.
[39] S.-C. Jin, Y.J. Kim, D.H. Lee, S.-H. Han, S. Jo, S.H. Park, Recrystallization behavior and microstructure evolution of Mg–5Bi–3Al alloy during very high-speed extrusion, Journal of Materials Science & Technology 191 (2024) 233–249, https://doi.org/10.1016/j.jmst.2023.11.074.
[40] M. Nienaber, G. Kurz, D. Letzig, K.U. Kainer, J. Bohlen, Effect of Process Temperature on the Texture Evolution and Mechanical Properties of Rolled and Extruded AZ31 Flat Products, Crystals 12 (2022) 1307, https://doi.org/10.3390/cryst12091307.
[41] J.-H. Peng, Z. Zhang, H.-H. Cheng, H.-G. Wei, L.-Y. Chen, Q.-H. Zang, S. Lu, J. Alloys Compd. 960 (2023) 170738, https://doi.org/10.1016/j.jallcom.2023.170738.
[42] D.R. Cooper, J.M. Allwood, The influence of deformation conditions in solid-state aluminium welding processes on the resulting weld strength, J. Mater. Process. Technol. 214 (2014) 2576–2592, https://doi.org/10.1016/j.jmatprotec.2014.04.018.
[43] R. Armstrong, I. Codd, R.M. Douthwaite, N.J. Petch, The plastic deformation of polycrystalline aggregates, Philos. Mag. 7 (1962) 45–58, https://doi.org/10.1080/14786436208201857.
[44] E.O. Hall, The Deformation and Ageing of Mild Steel: III Discussion of Results, Proc. Phys. Soc. B 64 (1951) 747–753, https://doi.org/10.1088/0370-1301/64/9/303.
[45] N.J. Petch, The cleavage strength of polycrystals, J. Iron Steel Inst. 174 (1953) 25–28.
[46] S.M. Razavi, D.C. Foley, I. Karaman, K.T. Hartwig, O. Duygulu, L.J. Kecskes, S. N. Mathaudhu, V.H. Hammond, Effect of grain size on prismatic slip in Mg–3Al–1Zn alloy, Scripta Materialia 67 (2012) 439–442, https://doi.org/10.1016/j.scriptamat.2012.05.017.
[47] H. Yu, Y. Xin, M. Wang, Q. Liu, Hall-Petch relationship in Mg alloys: A review, Journal of Materials Science & Technology 34 (2018) 248–256, https://doi.org/10.1016/j.jmst.2017.07.022.
[48] J. Hirsch, T. Al-Samman, Superior light metals by texture engineering: Optimized aluminum and magnesium alloys for automotive applications, Acta Mater. 61 (2013) 818–843, https://doi.org/10.1016/j.actamat.2012.10.044.
[49] J. Bohlen, S. Yi, D. Letzig, K.U. Kainer, Effect of rare earth elements on the microstructure and texture development in magnesium–manganese alloys during extrusion, Mater. Sci. Eng., A 527 (2010) 7092–7098, https://doi.org/10.1016/j.msea.2010.07.081.
[50] J. Bohlen, S.B. Yi, J. Swiostek, D. Letzig, H.G. Brokmeier, K.U. Kainer, Microstructure and texture development during hydrostatic extrusion of magnesium alloy AZ31, Scr. Mater. 53 (2005) 259–264, https://doi.org/10.1016/j.scriptamat.2005.03.036.